

Photoelectron velocity map imaging spectroscopic and theoretical study of heteronuclear vanadium-nickel carbonyl anions VNi(CO)_n^- ($n = 2-6$)

Qinqin Yuan, Jumei Zhang, Jinghan Zou, Hongjun Fan, Ling Jiang, and Hua Xie

Citation: *The Journal of Chemical Physics* **149**, 144305 (2018); doi: 10.1063/1.5050836

View online: <https://doi.org/10.1063/1.5050836>

View Table of Contents: <http://aip.scitation.org/toc/jcp/149/14>

Published by the [American Institute of Physics](#)

Articles you may be interested in

[Probing the structures and bonding of auropolynes, \$\text{Au}-\(\text{C}\equiv\text{C}\)_n-\text{Au}^-\$ \(\$n = 1-3\$ \), using high-resolution photoelectron imaging](#)

The Journal of Chemical Physics **149**, 144307 (2018); 10.1063/1.5040336

[Photoionization of the iodine 3d, 4s, and 4p orbitals in methyl iodide](#)

The Journal of Chemical Physics **149**, 144302 (2018); 10.1063/1.5035496

[Vacuum ultraviolet excited state dynamics of the smallest ring, cyclopropane. II. Time-resolved photoelectron spectroscopy and ab initio dynamics](#)

The Journal of Chemical Physics **149**, 144311 (2018); 10.1063/1.5044402

[Perspective: The development and applications of H Rydberg atom translational spectroscopy methods](#)

The Journal of Chemical Physics **149**, 080901 (2018); 10.1063/1.5047911

[Vacuum ultraviolet excited state dynamics of the smallest ring, cyclopropane. I. A reinterpretation of the electronic spectrum and the effect of intensity borrowing](#)

The Journal of Chemical Physics **149**, 144310 (2018); 10.1063/1.5044392

[DAVIS: A direct algorithm for velocity-map imaging system](#)

The Journal of Chemical Physics **148**, 194101 (2018); 10.1063/1.5025057

PHYSICS TODAY

WHITEPAPERS

ADVANCED LIGHT CURE ADHESIVES

Take a closer look at what these environmentally friendly adhesive systems can do

READ NOW

PRESENTED BY
 MASTERBOND
ADHESIVES | SEALANTS | COATINGS

Photoelectron velocity map imaging spectroscopic and theoretical study of heteronuclear vanadium-nickel carbonyl anions $\text{VNi}(\text{CO})_n^-$ ($n = 2-6$)

Qinqin Yuan,^{1,2} Jumei Zhang,^{1,2} Jinghan Zou,^{1,2} Hongjun Fan,¹ Ling Jiang,^{1,a)} and Hua Xie^{1,a)}

¹State Key Laboratory of Molecular Reaction Dynamics, Dalian Institute of Chemical Physics, Chinese Academy of Sciences, 457 Zhongshan Road, Dalian 116023, China

²University of Chinese Academy of Sciences, 19A Yuquan Road, Beijing 100049, China

(Received 3 August 2018; accepted 20 September 2018; published online 9 October 2018)

Mass-selected heteronuclear vanadium-nickel carbonyl anions $\text{VNi}(\text{CO})_n^-$ ($n = 2-6$) were investigated by photoelectron velocity-map imaging spectroscopy and quantum chemical calculations to obtain their chemical bonding and intrinsic electronic structure in the gas phase. The calculated energies (adiabatic detachment energies)/vertical detachment energies (VDEs) match well with experimental values: 1.30/1.49, 1.66/1.95, 2.22/2.48, 2.70/2.89, and 2.95/3.15 eV. The VDE value of $\text{VNi}(\text{CO})_n^-$ increases with an increase of cluster size, implying that the negative electron is stabilized upon the bonding of CO molecules. $\text{VNi}(\text{CO})_2^-$ consists of one bridging carbonyl and one terminal carbonyl, whose feature is different from $\text{MNi}(\text{CO})_2^-$ ($M = \text{Sc}, \text{Y}, \text{La}, \text{and Ce}$) with the involvement of one side-on-bonded carbonyl and one terminal CO carbonyl. The building block composed of three bridging carbonyls is favored for $\text{VNi}(\text{CO})_3^-$, the structure of which persists up to $n = 6$. The additional CO ligands are preferentially coordinated in the terminal mode to the Ni atom at $n = 4$ and then to the V atom at $n = 5$ and 6. The results obtained in this work would provide a molecular-level understanding about chemisorbed CO molecules on alloy surfaces/interfaces, which is important to understand CO molecule activation processes. *Published by AIP Publishing.*
<https://doi.org/10.1063/1.5050836>

I. INTRODUCTION

The interaction between transition metals (TM) and carbon monoxide has unique applications in heterogeneous and homogeneous catalysis, inorganic, organometallic, and coordination chemistry, which often takes place at solutions and interfaces.¹⁻³ Recently, the interaction of the single CO molecule with transition metal in the gas-phase, typically in the size range of 3 to more than 20 atoms, has been compared to the behavior of CO adsorbed on extended surfaces in a review.⁴ Fundamental understanding of the chemical environment for this related simply prototypical model (TM carbonyl anions) in the gas phase is of great scientific and practical interest to deduce the multifaceted mechanisms of CO chemisorption on metal surfaces and the binding at active sites of the catalyst at the molecular level. In recent decades, TM carbonyl clusters were investigated by various kinds of spectroscopic technological and theoretical methods: collision-induced dissociation coupled with mass spectrometry,⁵⁻⁷ Raman and infrared (IR) spectroscopy,⁸⁻¹¹ Fourier-transform microwave spectroscopy,¹² and photoelectron spectroscopy (PES)¹³⁻¹⁶ to obtain the information about the electronic structures, vibrational frequencies, bond energies, and so on.

Mononuclear metal carbonyl clusters have been the subject of extensive studies for more than a century since

the first report of $\text{Ni}(\text{CO})_4$ in 1890,¹⁷ revealing that the particular two bonding modes ($M \leftarrow \text{CO}$: σ -donation and $M \rightarrow \text{CO}$: π -back donation) between terminal carbonyls and metal.^{18,19} Homobinuclear and heterobinuclear metal carbonyl clusters have gained increasing attention and have also been studied theoretically and experimentally. Theoretical studies of the chemical environment of one CO with homobinuclear TM across the 3d series have revealed that the preference for bonding mode of M_2CO is from side-on-bonded to bridging, and then to terminal, whereas Ni_2CO prefers bridging configuration,¹¹ which was partly confirmed by experiments.²⁰⁻²² Several homobinuclear TM multi-carbonyl clusters have been observed to exhibit unusual bonding models. The $\text{Ti}_2(\text{CO})_n^-$ ($n = 4-6$) series contain side-on-bonded and terminal carbonyls.²³ The third CO in $\text{Au}_2(\text{CO})_3^-$ is weakly bonded with a linear $\text{Au}_2(\text{CO})_2^-$ core, forming physisorbed complexes.²² The $\text{Cr}_2(\text{CO})_n^+$ ($n = 7-9$) cations have the $(\text{OC})_5\text{Cr}-\text{C}-\text{O}-\text{Cr}(\text{CO})_{n-6}^+$ structures with a linear bridging carbonyl group between two Cr atoms.²⁴ The saturated cluster $\text{Fe}_2(\text{CO})_8^-$, $\text{Co}_2(\text{CO})_8^+$, and $\text{Cu}_2(\text{CO})_6^+$ preferably possessed $(\text{OC})_4\text{Fe}-\text{Fe}(\text{CO})_{n-4}^-$, $(\text{OC})_4\text{Co}-\text{Co}(\text{CO})_4^+$, and $(\text{OC})_3\text{Cu}-\text{Cu}(\text{CO})_3^+$ structures with all terminal carbonyls, then the preference for bonding mode of extra CO is around the saturated building block.²⁵⁻²⁷ $\text{Co}_2(\text{CO})_9^+$ has a mixture of the CO-tagged $\text{Co}_2(\text{CO})_8^+-\text{CO}$ complex and the $\text{Co}(\text{CO})_5^+-\text{Co}(\text{CO})_4$ ion-molecular complex.²⁶

For the heterobinuclear metal carbonyl clusters, infrared photodissociation spectroscopic (IRPD) studies have revealed

^{a)}Electronic addresses: ljjiang@dicp.ac.cn and xiehua@dicp.ac.cn

that the $M\text{Fe}(\text{CO})_8^+$ ($M = \text{Co}, \text{Ni}, \text{Cu}$) complexes have eclipsed $(\text{CO})_5\text{Fe}-\text{M}(\text{CO})_3^+$ structures and $\text{MCu}(\text{CO})_7^+$ ($M = \text{Co}, \text{Ni}$) complexes have staggered $(\text{CO})_4\text{M}-\text{Cu}(\text{CO})_3^+$ structures, the $\text{FeZn}(\text{CO})_5^+$ complex has a $(\text{CO})_5\text{Fe}-\text{Zn}^+$ structure and the $\text{CoZn}(\text{CO})_7^+$ complex has a $(\text{CO})_4\text{Co}-\text{Zn}(\text{CO})_3^+$ structure.^{28,29} PES investigations of $\text{MNi}(\text{CO})_3^-$ ($M = \text{Mg}, \text{Ca}, \text{Al}, \text{Cu}$) have indicated that the three carbonyls are bonded terminally to the Ni atom, resulting in the formation of the $\text{Ni}(\text{CO})_3$ motif.^{30,31} In the $\text{PbFe}(\text{CO})_4^-$ clusters, the four carbonyls are bonded terminally to the Fe atom.³² In these heterobinuclear metal carbonyls aforementioned above, the main metal-CO coordination mode is terminal. Interestingly, the early transition metal-nickel carbonyl clusters, $\text{MNi}(\text{CO})_3^-$ ($M = \text{Sc}, \text{Y}, \text{La}, \text{Ce}, \text{Ti}, \text{Zr}, \text{Hf}$), possess three kinds of different CO modes (side-on-bonded, bridging, and terminal carbonyls), whose building block is persisted up to $n = 6$ only for Sc and Y.¹⁴⁻¹⁶

In the present work, we report a study on a series of heteronuclear vanadium-nickel carbonyl clusters $\text{VNi}(\text{CO})_n^-$ ($n = 2-6$). Photoelectron velocity-map imaging spectroscopic and theoretical investigations reveal that two CO bonding modes (bridging and terminal carbonyls) are involved in the $n = 2$ cluster. The building block composed of three bridging carbonyls is favored at $n = 3$, the structure of which persists up to $n = 6$. The additional CO ligands are preferentially coordinated in the terminal mode to the Ni atom at $n = 4$ and then to the V atom at $n = 5$ and 6.

II. EXPERIMENTAL AND THEORETICAL METHODS

The experiments were carried out using a homemade instrument which included a laser vaporization source and a dual-channel time-of-flight mass spectrometer (D-TOFMS) coupled with a velocity-map photoelectron imaging analyzer.³³ Details of the apparatus have been described elsewhere, and only a brief outline is given below. The heterodinuclear transition metal carbonyl anions were generated by a laser vaporization cluster source, and these cluster anions were obtained in a supersonic expansion of helium gas seeded with 5% CO. The typical stagnation pressure of the carrier gas was about 1-5 atm. The cluster anions were cooled and expanded into the source chamber. The anions of interest were mass selected by a McLaren Wiley time-of-flight spectrometer and then introduced into the photodetachment region. The photon energies of 355 nm (3.496 eV) and 266 nm (4.661 eV) were used for the photodetachment of these anionic clusters. The photoelectrons were detected by a micro-channel plate (MCP)/phosphor screen combination, and the resulting photoelectron images were collected using a charge-coupled device (CCD) camera. Each image was obtained by accumulating 10 000–50 000 laser shots at a 10 Hz repetition rate. The obtained raw image stood for the projection of the photoelectron density in the 3D laboratory frame onto the 2D imaging detector. The original 3D distribution was reconstructed using the Basis Set Expansion (BASEX) inverse Abel transform method, and the photoelectron spectrum was acquired. The photoelectron spectra were calibrated using the known spectrum of Au^- . The energy resolution was better than 5%,

corresponding to 50 meV at an electron kinetic energy (eKE) of 1 eV.

In order to elucidate the electronic and geometrical structures of $\text{VNi}(\text{CO})_n^{0/-1}$, theoretical calculations were performed using the Gaussian 09 programs.³⁴ The BP86 function was employed for the transition metal carbonyl clusters. The Aug-cc-pVTZ basis set was used for the C and O atoms,³⁵ and the SDD (SC-RECP, MWB28) basis set was used for the V and Ni atoms.³⁶ Harmonic frequency analysis was carried out to ensure that the obtained structures were real minima on the potential energy surfaces. Theoretically, the vertical detachment energy (VDE) was calculated as the difference in energy between the neutral and anionic species based on the optimized anionic geometry, and the adiabatic detachment energy (ADE) was calculated as the difference in energy between the neutral and the anion both at their optimized geometries. Relative energies and the ADEs included the zero-point-energy corrections.

III. RESULTS AND ANALYSIS

A. Photoelectron spectroscopy

Figures 1 and 2 show the photoelectron imaging results of $\text{VNi}(\text{CO})_n^-$ ($n = 2-6$) at 355 nm (3.496 eV) and 266 nm (4.661 eV), respectively. The raw images (black background) collected in the experiments indicate the projection of the 3D laboratory frame photoelectron probability density onto the plane of the imaging detector, and the reconstructed images (purple background) represent the central slice of the 3D distribution from its 2D projection. The direction of laser polarization is indicated by a double arrow on each raw image.

The single photon energy of 355 nm (3.496 eV) for $\text{VNi}(\text{CO})_n^-$ ($n = 2-6$) allows all ground states and some excited states of these compounds to be observed, as shown in Fig. 1. The photoelectron spectra mainly reveal an intense X band, and the VDE values of $\text{VNi}(\text{CO})_n^-$ ($n = 2-6$) are estimated from their band maxima in the 355 nm spectra to be 1.49 ± 0.10 , 1.95 ± 0.08 , 2.48 ± 0.05 , 2.89 ± 0.03 , and 3.15 ± 0.02 eV (Table I), respectively. The ADE values are estimated by drawing a straight line at the rising edge of the main band and then adding the instrumental resolution to the intersection with the binding energy axis. The ADE values of $\text{VNi}(\text{CO})_n^-$ ($n = 2-6$) are evaluated to be 1.30 ± 0.11 , 1.66 ± 0.09 , 2.22 ± 0.06 , 2.70 ± 0.04 , and 2.95 ± 0.03 eV (Table I), respectively. In the 266 nm spectra of $\text{VNi}(\text{CO})_n^-$ ($n = 2-6$) (Fig. 2), the intensities of the bands of ground states are relatively weaker and more excited states are present as compared to the 355 nm spectra.

B. Comparison between experimental and theoretical results

Optimized structures of $\text{VNi}(\text{CO})_n^-$ ($n = 2-6$) are illustrated in Fig. 3. None of the triplet anions are found to be energetically competitive with the corresponding singlet isomers. Accordingly, only the results of the representative low-energy isomers with the singlet electronic state are shown for

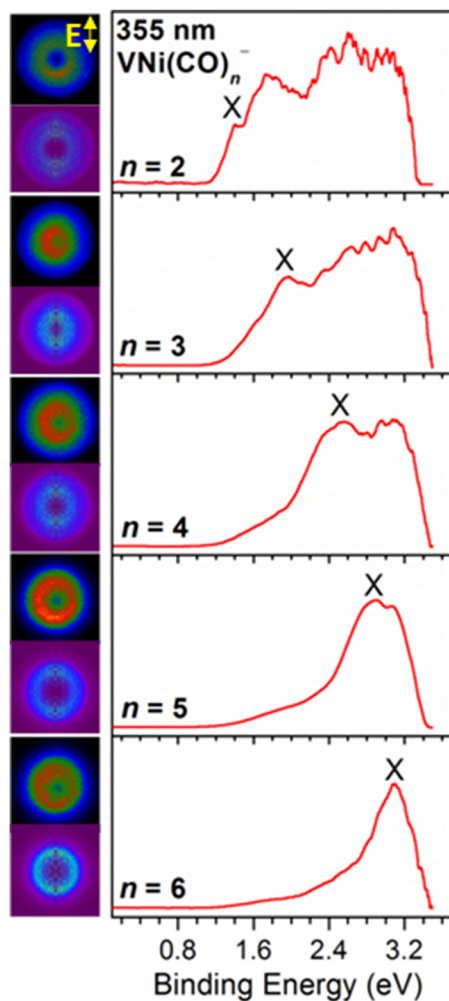


FIG. 1. Photoelectron images of $\text{VNi}(\text{CO})_n^-$ ($n = 2-6$) at 355 nm. The raw image (top) and the reconstructed image (bottom) after inverse Abel transformation are shown on the left side. The double arrow indicates the direction of the laser polarization. Photoelectron spectra are shown on the right side.

the present discussions. Table I lists the comparison of experimental VDE and ADE values to the BP86 calculated ones of the four lowest-energy isomers for $\text{VNi}(\text{CO})_n^-$ ($n = 2-6$), respectively.

1. $\text{VNi}(\text{CO})_2^-$

In Fig. 3, the lowest-lying isomer (labeled 2A) of $\text{VNi}(\text{CO})_2^-$ is a C_1 structure with a 1A ground state, in which two types of coordination configurations (i.e., bridging and terminal) are simultaneously involved and the terminal CO is bonded to the V atom. The second isomer (2B) has two bridging CO molecules and lies higher in energy above 2A by 0.18 eV. The 2C isomer (+0.45 eV) consists of two side-on-bonded carbonyls. The 2D isomer lies higher in energy above 2A by 0.57 eV, which has one side-on-bonded carbonyl and one terminal carbonyl. As listed in Table I, the calculated VDE of 2A (1.41 eV) is consistent with the experimental value of 1.49 ± 0.10 eV. The agreement of the calculated ADE value (1.22 eV) with the experimental value (1.30 ± 0.11 eV) is also obtained for the 2A isomer (Table I). The calculated VDEs and ADEs of isomers 2B-2E are largely deviated from the

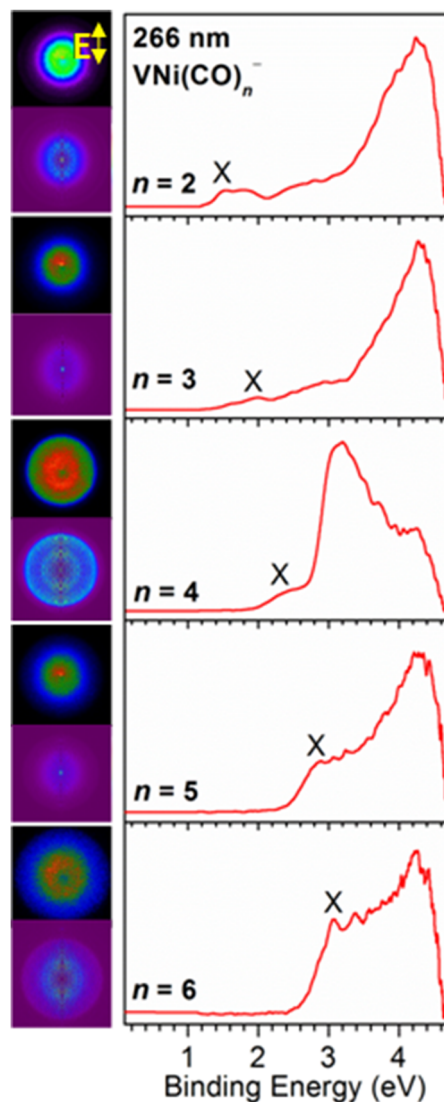


FIG. 2. Photoelectron images of $\text{VNi}(\text{CO})_n^-$ ($n = 2-6$) at 266 nm. The raw image (top) and the reconstructed image (bottom) after inverse Abel transformation are shown on the left side. The double arrow indicates the direction of the laser polarization. Photoelectron spectra are shown on the right side.

experimental values (Table I). It can be seen from Fig. 4 that the band positions and overall pattern of the simulated spectrum of the 2A isomer agree well with the experiment, suggesting that the 2A isomer should be responsible for the $n = 2$ spectrum.

2. $\text{VNi}(\text{CO})_3^-$

The lowest-energy isomer of $\text{VNi}(\text{CO})_3^-$ (3A) is exhibited by a C_s structure with a $^1A'$ ground state and consists of three bridging carbonyls (Fig. 3). The 3B isomer has two bridging carbonyls and one terminal carbonyl, which lies higher in energy above 3A by 0.38 eV. The 3C isomer (+0.56 eV) consists of one side-on-bonded carbonyl, one bridging carbonyl, and one terminal carbonyl. The 3D isomer (+1.00 eV) has two side-on-bonded carbonyls and one terminal carbonyl. The calculated VDE and ADE values for the most stable isomer 3A (1.80 and 1.59 eV) are consistent with the experimental values of 1.95 ± 0.08 and 1.66 ± 0.09 eV (Table I). However, the calculated VDE and ADE values for the 3B isomer (1.75 and

TABLE I. Comparison of experimental VDE and ADE values to the BP86 calculated ones of the four lowest-energy isomers for $\text{VNi}(\text{CO})_n^-$ ($n = 2-6$).

Cluster	Isomer	Relative energy (eV)	VDE (eV)		ADE (eV)	
			Expt. ^a	Calc.	Expt. ^a	Calc.
$n = 2$	2A	0.00	1.49(10)	1.41	1.30(11)	1.22
	2B	0.18		1.18		0.89
	2C	0.45		1.71		1.54
	2D	0.57		0.98		0.72
$n = 3$	3A	0.00	1.95(8)	1.80	1.66(9)	1.59
	3B	0.38		1.75		1.54
	3C	0.56		1.67		1.61
	3D	1.00		1.66		1.52
$n = 4$	4A	0.00	2.48(5)	2.59	2.22(6)	2.37
	4B	0.64		2.33		2.15
	4C	0.71		2.87		2.69
	4D	0.73		2.35		2.19
$n = 5$	5A	0.00	2.89(3)	3.13	2.70(4)	2.89
	5B	0.47		3.19		2.90
	5C	0.75		2.82		2.47
	5D	0.82		2.88		2.60
$n = 6$	6A	0.00	3.15(2)	3.40	2.95(3)	3.19
	6B	0.29		3.51		3.24
	6C	0.91		3.15		2.84
	6D	1.36		3.14		2.64

^aNumbers in parentheses represent the uncertainty in the last digit.

1.54 eV) are also close to the experimental values. As shown in Fig. 4, the simulated spectra of 3A and 3B are very similar and most of the bands were observed in the experimental spectrum. The band positions and overall pattern of the simulated spectrum of 3A is in slightly better agreement with the experiment but the presence of 3B cannot be ruled out.

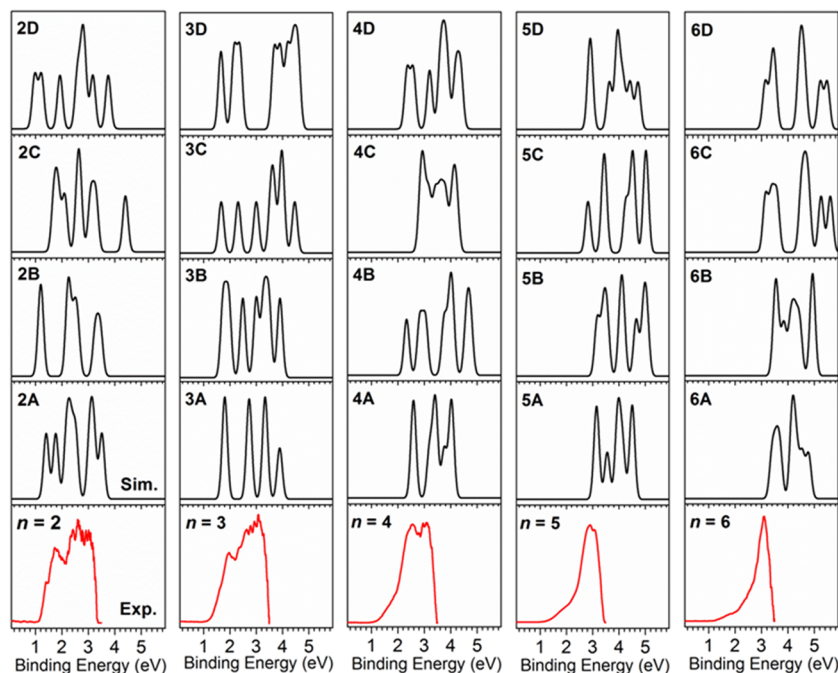


FIG. 4. Comparison of experimental 355 nm photoelectron spectra (bottom rows) of $\text{VNi}(\text{CO})_n^-$ ($n = 2-6$) to the simulated spectra of the nA - nD isomers (top rows).

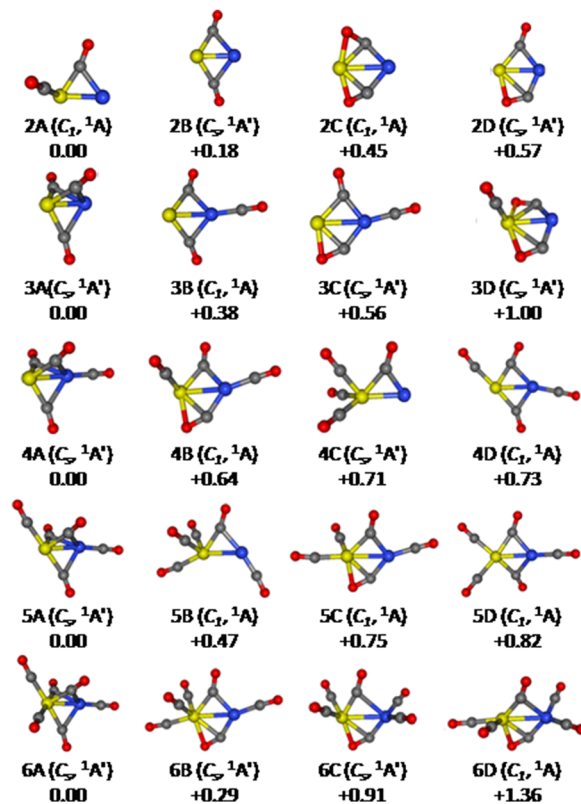


FIG. 3. Optimized structures of the four lowest-energy isomers for $\text{VNi}(\text{CO})_n^-$ ($n = 2-6$) (V, yellow; Ni, blue; C, gray; O, red). Relative energies are given in eV.

3. $\text{VNi}(\text{CO})_4^-$

For the $n = 4$ cluster, the lowest-energy isomer of $\text{VNi}(\text{CO})_4^-$ (4A) is a C_s structure with a $^1A'$ ground state (Fig. 3), which consists of three bridging carbonyls and one terminal carbonyl. The 4A structure could be viewed as being

derived from 3A by terminally bonding the fourth CO molecule to the Ni atom. The 4B isomer (+0.64 eV) has a C_1 structure with one side-on-bonded CO, one bridging CO, and two terminal carbonyls. The 4C isomer has one bridging and three terminal carbonyls, in which the three terminal carbonyls are bonded to the V atom. The 4D isomer has two bridging and two terminal carbonyls. The calculated VDE and ADE values of 4A (2.59 and 2.37 eV) agree with the experimental values of 2.48 ± 0.05 and 2.22 ± 0.06 eV (Table I). The experimental 355 nm spectrum is also reproduced by the simulated spectrum of 4A (Fig. 4). The 4B-4D isomers should lie too high in energy to be probed in the present experiment. The main contribution for the $n = 4$ spectrum should be from the 4A isomer.

4. $VNi(CO)_5^-$

The lowest-energy isomer of $VNi(CO)_5^-$ (5A) has three bridging carbonyls and two terminal carbonyls (Fig. 3), in which one terminal carbonyl is bonded to the V atom and another terminal carbonyl is bonded to the Ni atom. The 5B isomer has one bridging carbonyl, three terminal carbonyls bonded to the V atom, and one terminal carbonyl bonded to the Ni atom, which lies 0.47 eV higher in energy than the 5A isomer. The 5C isomer (+0.75 eV) has one side-on-bonded, one bridging, and three terminal carbonyls. The 5D isomer has two bridging and three terminal carbonyls, which lies 0.82 eV higher in energy than the 5A isomer. The calculated VDE and ADE values of the 5A isomer are consistent with the experimental values (Table I). The main feature of the experimental 355 nm spectrum is observed in the simulated spectrum of 5A (Fig. 4).

5. $VNi(CO)_6^-$

For the $n = 6$ cluster, the lowest-lying isomer of $VNi(CO)_6^-$ (6A) is indicated by a C_s structure with a ${}^1A'$ ground state (Fig. 3), which consists of three bridging and three terminal carbonyls, in which two terminal carbonyls are bonded to the V atom and one terminal carbonyl is bonded to the Ni atom. The 6C isomer (+0.29 eV) has one side-on-bonded, one bridging, three carbonyls terminally bonded to the V atom, and one carbonyl terminally bonded to the Ni atom. The third isomer (6C) lies 0.91 eV above 6A and consists of one side-on-bonded, one bridging, two carbonyls terminally bonded to the V atom, and two carbonyls terminally bonded to the Ni atom. The 6D isomer (+1.36 eV) has one side-on-bridging carbonyl, one bridging carbonyl, two carbonyls terminally bonded to the V atom, and two carbonyls terminally bonded to the Ni atom, slightly different from the 6C isomer. The calculated VDE and ADE values of the lowest-energy isomers for $VNi(CO)_6^-$ are in accord with the experimental values (Table I).

IV. DISCUSSION

The agreement between the experimental and theoretical results allows for establishing the structural evolution of $VNi(CO)_n^-$ ($n = 2-6$). As shown in Table I, the VDE value increases with an increase of cluster size, which implies that

the negative electron is stabilized upon sequential bonding of CO molecules. For $VNi(CO)_2^-$, the 2A isomer has one bridging carbonyl and one terminal carbonyl. The 3A structure only includes three bridging carbonyls, and the 4A isomer is derived from 3A by terminally bonding the fourth CO molecule to the Ni atom. The 5A and 6A structures are derived from 4A by continually terminal bonding the CO molecule to the V atom. In summary, two different kinds of CO bonding configurations (bridging and terminal carbonyls) are observed in the $n = 2$ cluster. The building block composed of three bridging CO carbonyls is favored at $n = 3$, the structure of which persists up to $n = 6$. The additional CO ligands are preferentially coordinated in the terminal mode to the Ni atom at $n = 4$ and then to the V atom at $n = 5$ and 6.

It can be found from the above analysis that $VNi(CO)_2^-$ is capable of accommodating two different coordination modes (i.e., bridging and terminal modes), which is quite different from the homobinuclear carbonyl $Ti_2(CO)_2^-$ with the involvement of two side-on-bonded CO ligands²³ and $Au_2(CO)_2^-$ and $CuNi(CO)_2^-$ with the involvement of two terminal CO ligands,^{22,30} and also discrepant from the heterobinuclear carbonyl $ScNi(CO)_2^-$ with the involvement of one side-on-bonded and one terminal CO ligands.¹⁵ The $VNi(CO)_3^-$ isomer only has three bridging CO bonding fashions, which is different from previous investigations of heterobinuclear metal-nickel carbonyl anions $MNi(CO)_3^-$ ($M = Sc, La, Ti, Cu$) including more than one coordinated styles.^{14-16,30} The geometry of the $VNi(CO)_4^-$ isomer is different from that of the $CuFe(CO)_4^-$ and $PbFe(CO)_4^-$ clusters in which all carbonyls are terminally bonded to the Fe atom.^{32,37} The building block of three bridging CO molecules in $VNi(CO)_n^-$ ($n = 4-6$) is similar to the previously reported $TiNi(CO)_n^-$ ($n = 4-6$) clusters.¹⁴ In $VNi(CO)_2^-$, the C–O bond distance in the bridging and terminal mode was calculated to be about 1.21 and 1.20 Å, respectively, which is longer than that of the free CO molecule (1.14 Å). The CO stretching frequency of the individual bridging and terminal carbonyl group in $VNi(CO)_2^-$ was predicted to be 1663 and 1701 cm^{-1} (unscaled), respectively, pointing to the strong and weak C–O bond activation. Generally, the bridging and terminal bonding of CO on the metal catalyst is a common feature. The $VNi(CO)_n^-$ ($n = 2-6$) systems reveal a rich fashion of metal-CO coordination covering from terminal to bridging mode, implying that the extent of C–O bond activation could be adjusted by tuning the cluster size. These findings would have important implications for understanding the CO activation and chemisorbed CO molecules on metal catalysts via the selection of different transition metals and metal compounds.

V. CONCLUSIONS

A series of heterobinuclear metal-nickel carbonyl anions $VNi(CO)_n^-$ ($n = 2-6$) have been generated via a laser vaporization supersonic cluster source and characterized by mass-selected photoelectron velocity-map imaging spectroscopy. Quantum chemical calculations have been carried out to elucidate the geometric and electronic structures and support the spectral assignments. Two CO bonding modes (bridging and terminal carbonyls) are involved in the $n = 2$ cluster. The

building block composed of three bridging carbonyls is favored at $n = 3$, the structure of which persists up to $n = 6$. The present findings provide important new insight into the structure and bonding mechanism of CO molecules with heteronuclear transition metals, which would have important implications for understanding the CO molecule activation and the chemisorbed CO molecules on alloy surfaces.

ACKNOWLEDGMENTS

This work was supported by the National Natural Science Foundation of China (Grant Nos. 21327901, 21503222, 21673231, and 21688102) and the Strategic Priority Research Program of the Chinese Academy of Sciences (Grant No. XDB17000000).

- ¹R. F. Heck, *Organotransition Metal Chemistry* (Academic Press, New York, 1974).
- ²J. E. Huheey, E. A. Keiter, and R. L. Keiter, *Inorganic Chemistry Principles of Structure and Reactivity* (Harper Collins, New York, 1993).
- ³F. A. Cotton, G. Wilkinson, C. A. Murillo, and M. Bochmann, *Advanced Inorganic Chemistry*, 6th ed. (John Wiley & Sons, New York, 1999).
- ⁴A. Fielicke, P. Gruene, G. Meijer, and D. M. Rayner, *Surf. Sci.* **603**, 1427 (2009).
- ⁵X.-G. Zhang and P. B. Armentrout, *Organometallics* **20**, 4266 (2001).
- ⁶L. Sunderlin, D. Wang, and R. R. Squires, *J. Am. Chem. Soc.* **114**, 2788 (1992).
- ⁷F. Meyer, Y.-M. Chen, and P. B. Armentrout, *J. Am. Chem. Soc.* **117**, 4071 (1995).
- ⁸M. Zhou and L. Andrews, *J. Chem. Phys.* **111**, 4548 (1999).
- ⁹B. Liang, M. Zhou, and L. Andrews, *J. Phys. Chem. A* **104**, 3905 (2000).
- ¹⁰Q. Xu and L. Jiang, *J. Phys. Chem. A* **110**, 2655 (2006).
- ¹¹L. Jiang and Q. Xu, *J. Chem. Phys.* **128**, 124317 (2008).
- ¹²T. Okabayashi, T. Yamamoto, E. Y. Okabayashi, and M. Tanimoto, *J. Phys. Chem. A* **115**, 1869 (2011).
- ¹³J. Reutt, L. Wang, Y.-T. Lee, and D. Shirley, *Chem. Phys. Lett.* **126**, 399 (1986).
- ¹⁴J. Zou, H. Xie, Q. Yuan, J. Zhang, D. Dai, H. Fan, Z. Tang, and L. Jiang, *Phys. Chem. Chem. Phys.* **19**, 9790 (2017).
- ¹⁵H. Xie, J. Zou, Q. Yuan, J. Zhang, H. Fan, and L. Jiang, *Top. Catal.* **61**, 71 (2018).
- ¹⁶G. Li, J. Zhang, H. Xie, X. Kong, and L. Jiang, *J. Phys. Chem. A* **122**, 3811 (2018).
- ¹⁷L. Mond, C. Langer, and F. Quincke, *J. Chem. Soc., Dalton Trans.* **57**, 749 (1890).
- ¹⁸A. J. Bridgeman, *Inorg. Chim. Acta* **321**, 27 (2001).
- ¹⁹M. Zhou, L. Andrews, and C. W. Bauschlicher, *Chem. Rev.* **101**, 1931 (2001).
- ²⁰L. Jiang and Q. Xu, *J. Phys. Chem. A* **110**, 5636 (2006).
- ²¹L. Jiang and Q. Xu, *J. Am. Chem. Soc.* **127**, 42 (2005).
- ²²Y.-L. Wang, H.-J. Zhai, L. Xu, J. Li, and L.-S. Wang, *J. Phys. Chem. A* **114**, 1247 (2009).
- ²³J. Zou, H. Xie, D. Dai, Z. Tang, and L. Jiang, *J. Chem. Phys.* **145**, 184302 (2016).
- ²⁴X. Zhou, J. Cui, Z. H. Li, G. Wang, and M. Zhou, *J. Phys. Chem. A* **116**, 12349 (2012).
- ²⁵C. Chi, J. Cui, Z. H. Li, X. Xing, G. Wang, and M. Zhou, *Chem. Sci.* **3**, 1698 (2012).
- ²⁶J. Cui, X. Zhou, G. Wang, C. Chi, Z. H. Li, and M. Zhou, *J. Phys. Chem. A* **118**, 2719 (2014).
- ²⁷J. Cui, X. Zhou, G. Wang, C. Chi, Z. Liu, and M. Zhou, *J. Phys. Chem. A* **117**, 7810 (2013).
- ²⁸H. Qu, F. Kong, G. Wang, and M. Zhou, *J. Phys. Chem. A* **120**, 7287 (2016).
- ²⁹H. Qu, F. Kong, G. Wang, and M. Zhou, *J. Phys. Chem. A* **121**, 1627 (2017).
- ³⁰Z. Liu, H. Xie, Z. Qin, H. Fan, and Z. Tang, *Inorg. Chem.* **53**, 10909 (2014).
- ³¹H. Xie, J. Zou, Q. Yuan, H. Fan, Z. Tang, and L. Jiang, *J. Chem. Phys.* **144**, 124303 (2016).
- ³²Z. Liu, J. Zou, Z. Qin, H. Xie, H. Fan, and Z. Tang, *J. Phys. Chem. A* **120**, 3533 (2016).
- ³³Z. B. Qin, X. Wu, and Z. C. Tang, *Rev. Sci. Instrum.* **84**, 066108 (2013).
- ³⁴M. J. Frisch, G. W. Trucks, H. B. Schlegel, G. E. Scuseria, M. A. Robb, J. R. Cheeseman, G. Scalmani, V. Barone, B. Mennucci, G. A. Petersson, H. Nakatsuji, M. Caricato, X. Li, H. P. Hratchian, A. F. Izmaylov, J. Bloino, G. Zheng, J. L. Sonnenberg, M. Hada, M. Ehara, K. Toyota, R. Fukuda, J. Hasegawa, M. Ishida, T. Nakajima, Y. Honda, O. Kitao, H. Nakai, T. Vreven, J. A. Montgomery, Jr., J. E. Peralta, F. Ogliaro, M. J. Bearpark, J. Heyd, E. N. Brothers, K. N. Kudin, V. N. Staroverov, R. Kobayashi, J. Normand, K. Raghavachari, A. P. Rendell, J. C. Burant, S. S. Iyengar, J. Tomasi, M. Cossi, N. Rega, N. J. Millam, M. Klene, J. E. Knox, J. B. Cross, V. Bakken, C. Adamo, J. Jaramillo, R. Gomperts, R. E. Stratmann, O. Yazyev, A. J. Austin, R. Cammi, C. Pomelli, J. W. Ochterski, R. L. Martin, K. Morokuma, V. G. Zakrzewski, G. A. Voth, P. Salvador, J. J. Dannenberg, S. Dapprich, A. D. Daniels, O. Farkas, J. B. Foresman, J. V. Ortiz, J. Cioslowski, and D. J. Fox, *GAUSSIAN 09*, Revision A.02, Gaussian, Inc., Wallingford, CT, USA, 2009.
- ³⁵T. H. Dunning, *J. Chem. Phys.* **90**, 1007 (1989).
- ³⁶M. Dolg, H. Stoll, and H. Preuss, *J. Chem. Phys.* **90**, 1730 (1989).
- ³⁷N. Zhang, M. Luo, C. Chi, G. Wang, J. Cui, and M. Zhou, *J. Phys. Chem. A* **119**, 4142 (2015).